

Mapping the core senescence phenotype of primary human colon fibroblasts

Namita Ganesh Hattangady¹, Kelly Carter¹, Brett Maroni-Rana¹, Ting Wang¹, Jessica Lee Ayers¹, Ming Yu¹, William M. Grady^{1,2,3}

¹Translational Science and Therapeutics Division, Fred Hutchinson Cancer Center, Seattle, WA 98109, USA

²Public Health Sciences Division, Fred Hutchinson Cancer Center, Seattle, WA 98109, USA

³Division of Gastroenterology, University of Washington School of Medicine, Seattle, WA 98195, USA

Correspondence to: William M. Grady, Ming Yu; **email:** wgrady@fredhutch.org, myu@fredhutch.org

Keywords: senescence, senescence associated secretory phenotype, SASP, colorectal cancer, cancer

Received: May 16, 2023

Accepted: January 15, 2024

Published: February 21, 2024

Copyright: © 2024 Hattangady et al. This is an open access article distributed under the terms of the [Creative Commons Attribution License](https://creativecommons.org/licenses/by/4.0/) (CC BY 4.0), which permits unrestricted use, distribution, and reproduction in any medium, provided the original author and source are credited.

ABSTRACT

Advanced age is the largest risk factor for many diseases and several types of cancer, including colorectal cancer (CRC). Senescent cells are known to accumulate with age in various tissues, where they can modulate the surrounding tissue microenvironment through their senescence associated secretory phenotype (SASP). Recently, we showed that there is an increased number of senescent cells in the colons of CRC patients and demonstrated that senescent fibroblasts and their SASP create microniches in the colon that are conducive to CRC onset and progression. However, the composition of the SASP is heterogenous and cell-specific, and the precise senescence profile of colon fibroblasts has not been well-defined. To generate a SASP atlas of human colon fibroblasts, we induced senescence in primary human colon fibroblasts using various *in vitro* methods and assessed the resulting transcriptome. Using RNAsequencing and further validation by quantitative RT-PCR and Luminex assays, we define and validate a 'core senescent profile' that might play a significant role in shaping the colon microenvironment. We also performed KEGG analysis and GO analyses to identify key pathways and biological processes that are differentially regulated in colon fibroblast senescence. These studies provide insights into potential driver proteins involved in senescence-associated diseases, like CRC, which may lead to therapies to improve overall health in the elderly and to prevent CRC.

INTRODUCTION

Advanced age is by far the highest risk factor for many diseases such as atherosclerosis, diabetes, macular degeneration, neurodegenerative diseases, and several types of cancers, including colorectal cancer (CRC) [1]. Aging and age-associated pathologies are associated with several biological and molecular alterations that affect a variety of cell processes including cellular metabolism, inflammatory responses, proteostasis, and regulation of the epigenome. One of the most common age-related phenomena seen in various tissues and across various species is the accumulation of senescent

cells. Cellular senescence, as described by Hayflick, is a state of irreversible arrest of cell proliferation [2]. It is characterized by the accumulation of DNA damage, induction of p53/p21 and/or p16^{INK4a}/pRB tumor suppressive pathways, elevated senescence associated Beta-galactosidase activity at pH6, senescence-associated heterochromatin foci and morphological changes such as enlargement and flattening of cells, and the increased appearance of vacuoles [3–5]. A significant feature of senescent cells, first described in 2008 by Campisi and colleagues [6], is the production of a complex senescence associated secretory phenotype (SASP) that consists of hundreds of secreted proteins including

cytokines, chemokines and growth factors. As a result of the SASP, senescent cells can modulate the surrounding tissue microenvironment, promote embryonic development, remodel the extracellular matrix, enable wound healing, and activate tumor-suppressive pathways, even in young individuals [3, 7–10]. In nonpathological states, senescent cells are cleared from healthy tissues when the inciting event is resolved [3, 8–11]. However, the persistent increase in senescent cell numbers seen in tissues of the elderly appears to lead to chronic inflammation, which can induce pro-tumorigenic pathways being activated as well age-related functional decline [12–17]. *In vivo* and *in vitro* studies confirm that removal of senescent cells, and thereby reducing SASP, can prevent or slow the onset of age-related pathologies [18–20]. However, the composition of SASP is cell-specific, and heterogenous, differing based on the senescence triggering agent [21–26].

In the context of CRC, we recently showed that an increased number of senescent fibroblasts is present in the normal healthy colons of subjects with concurrent CRC [12] and hypothesized that their SASP may alter the colon tissue microenvironment to create microniches that are conducive to CRC onset and progression. Our *in vitro* studies have already demonstrated that SASP from oxidative stress-induced senescence in colon fibroblasts can activate cancer hallmark molecular pathways and behaviors such as proliferation, migration and invasion in normal epithelial cells and benign and malignant neoplastic cell lines. Besides oxidative stress, the colon tissue microenvironment is rich in several genotoxic stressors due to the presence of toxic by-products of consumed food, dysbiosis of microbiota, secreted microbial toxins, etc., which have the potential to induce a unique senescent profile and SASP's in colon fibroblasts. The senescent signatures of various cell types and established cell lines [21, 23–28], including dermal, pulmonary, neuronal and bone marrow cells, has revealed that each cell type has a unique SASP, with some components that are common to a universal senescent cell signature and others that are unique. Notably, despite the impact of aging on colon health and colon cancer, an atlas of the SASP produced by colon fibroblasts has not been established.

To address this gap in knowledge, we utilized various relevant stressors to induce senescence in primary cultures of colon fibroblasts and perform RNA sequencing (RNASeq) to define an atlas of stressor-specific senescent profiles and a core senescent profile that is commonly regulated by all senescence inducers. We validated six of eight core senescent candidates in the transcriptome by qPCR and in the secretome by a Luminex assay. We also defined enriched pathways, biological processes and molecular functions that are

characteristic of the core senescent profile in colon fibroblasts.

MATERIALS AND METHODS

Primary fibroblast isolation

The normal healthy rectosigmoid colon adjacent to concurrent tumor was collected during surgical resection of tumor after informed consent through the IRB approved ColoCare Study, as previously described [12]. Participants consisted of men and women aged 43 years to 71 years old (Supplementary Table 1). Each colon tissue was cut into small (1–2 mm) fragments and washed with cold DPBS three times. The tissue fragments were transferred into a 50 ml conical tube and incubated with 25 ml HBSS (without Ca^{2+} and Mg^{2+}) with 5 mM EDTA at 37°C in shaking air bath (250 rpm) for 1.5 hours to denude the fragments. After a wash in cold DPBS, the fragments were incubated with 20 ml HBSS (without Ca^{2+} and Mg^{2+}) with 2000 U of collagenase D and 20 U of Dispase at 37°C in a shaking air bath (250 rpm) for 1 hour. The isolated cells were centrifuged ($200 \times g$ at 4°C for 5 min) and resuspended with EMEM medium with 10% fetal bovine serum and 1% penicillin-streptomycin. The resuspended cells were strained through a 70 μm cell strainer and incubated in TC-treated T25 flasks at 37°C in 5% oxygen. After overnight incubation, the cells were washed gently with EMEM medium. The adherent cells include epithelial cells and fibroblasts, with only the fibroblast cells surviving the first passage. Fibroblasts were cultured for 4–6 Population Doublings (PD) prior to use for senescence induction.

Senescence induction and detection

For senescence induction, primary human colon fibroblasts were plated on day 0 at a density of 100,000 cells/well in a 6-well plate and allowed to adhere for 24 hours. Senescence was induced in primary cultures of human colon fibroblasts using three different stressors – hydrogen peroxide, doxorubicin and bleomycin. For oxidative stress-induced senescence, cells were treated with 400 μM hydrogen peroxide (30% w/v Sigma Aldrich) for 2 hours on day 1, followed by media removal, three 30 second-washes in 1X DPBS and recovery in growth media for 2 days. This treatment was repeated on days 4 and 7. For doxorubicin induced senescence, cells were incubated with 250 nM doxorubicin for 24 hours, then media was discarded, cells were washed three times in 1X DPBS and recovered in growth media for 9 days. For bleomycin induced senescence, cells were treated with 10 ng/mL bleomycin sulphate for 3 hours. At the end of treatment, cells were washed

in DPBS and recovered with media changes, as needed, until day 10. The cellular morphology was observed daily and cells were split in a 1:2 ratio cells were >90% confluent. Proliferating cells with the same number of PD's treated with vehicle were used as control. At the end of recovery from each treatment, on day 10, cells were plated for senescence detection and harvested for RNA isolation if >80% cells were senescent. Senescence was confirmed using the commercially available senescence associated B-gal assay kit (Biovision, Milpitas, CA, USA #K320-250) as per manufacturer recommendations. Cells plated in 24-well plates were fixed and incubated overnight in X-gal solution. At the end of 16 hours of incubation, the cells were washed first with PBS, methanol at room temperature and air dried in a dark room. The number of SA- β -gal positive cells were counted using ImageJ 1.5i using the multi-point tool.

RNA isolation and RNASeq analysis

RNA was isolated from pelleted cells using TRIzol. Briefly, cell pellets were resuspended in 2–3 mL of TRIzol and homogenized using a 3 mL syringe and a 0.8 × 25 mm gauge needle. Samples were incubated at RT for 5 mins, 0.2 mL chloroform was added to each tube and shaken vigorously. Samples were incubated at room temperature for 2–3 mins, centrifuged at 4°C for 15 mins at maximum speed. The clear aqueous layer was transferred to a clean centrifuge tube, ensuring that none of the buffy coat was not included. One microliter glycogen and 0.5 mL isopropanol were added to each tube followed by vigorous shaking. After incubation for 10 mins at 4°C, RNA was pelleted by centrifugation at maximum speed for 10 mins. The RNA pellet was washed with 75% ethanol three times. After the last wash, the pellet was dried on a heat block at 55°C for 10 mins. After cooling to room temperature, the RNA was resuspended in nuclease free water and measured using nanodrop. RNA was cleaned using sodium acetate to ensure an acceptable 260/280 ratio with 260/280 ratios more than 1.9. RNA quality was confirmed using the Agilent 4200 TapeStation. A hundred nanograms from each of the non-senescent and senescent primary colon fibroblast cells (derived from three subjects and induced into senescence using oxidative or genotoxic stress) were prepared at 10 ng/mL in nuclease free water Library preparation and RNASequencing was performed by the Genomics and Bioinformatics Core at the Fred Hutchinson Cancer Center. Libraries were prepared using TruSeq Stranded mRNA (Illumina, San Diego, CA, USA) and sequencing was performed at a depth of 30 M reads/sample with 50 paired end reads/cycle using a P2 flow cell on the NextSeq2000 Sequencing system (Illumina, San Diego, CA, USA).

Analysis of the RNA-seq data

Quality control for raw fastq files were performed with FastQC [29] and MultiQC, the low-quality reads and 3' adapters were trimmed with Trim Galore! [30] and Cutadapt [31]. Then the trimmed reads were aligned to reference human genome (hg38) with the RNA-seq aligner STAR [32]. Subsequently, gene expression for each sample was quantified by counting the number of read fragments that were uniquely mapped to genes using the RSEM [33]. Genes with average read count <5 were firstly filtered out. Differential expression (DE) analysis was performed using the R package DESeq2 [34], and the genes with FDR <0.01 and log₂ (Fold Change over non-senescent cells (NS) as control cells) >1 were considered as significantly up-regulated genes.

Pathway and gene set analyses

The enrichment of DEGs in KEGG pathways was analyzed using the R package Limma [35] and the 'Kegga' function while the enrichment of DEGs in GO terms was analyzed using ShinyGO v0.76. An enrichment for secreted proteins in the core senescent profile versus the total transcriptome was identified by generating the number of transcripts coding for secreted proteins in a randomly chosen set of one thousand transcripts from each of the genelists, for the total transcriptome consisting of 15569 transcripts, this was repeated a total of three times. The enrichment of secreted proteins in the core senescent profile was confirmed by Fisher's Exact test [36].

Data visualization

Volcano plots were visualized in R using the 'EnhancedVolcano' package. KEGG enrichment analysis was plotted in R using the 'ggplot2'. The gene ratio was calculated by dividing the number of DEGs in our dataset by the total number of genes in a particular pathway. This was plotted along the x-axis with FDR adjusted *p*-value represented by color and the number of DEGs found represented by size. GO term enrichment was visualized using the 'pheatmap' package. Hierarchical clustering was applied to the GO term and its associated log₂FC to cluster GO terms with similar log₂FC. The package 'RColorBrewer' was used to generate color palettes.

Synthesis of cDNA and quantitative real-time PCR analysis

RNA concentrations were measured at 260 nm using NanoDrop (Thermo Fisher Scientific, Waltham, MA, USA). The cDNA was synthesized using iScript™ cDNA Synthesis Kit (Bio-Rad, Hercules, CA, USA)

according to manufacturer's instructions. Quantitative real-time quantitative PCR was performed using predesigned primer-probe sets (Thermo Fisher Scientific) for the various transcripts, including GAPDH which was used for normalization of gene expression levels. All quantitative real-time PCR were performed via a CFX96 Touch Real-Time PCR Detection System (Bio-Rad) and results were analyzed using CFX Manager software, version 3.1 (Bio-Rad). GAPDH (pre-designed primer-probe set) was used for normalization of cDNA loading between samples and fold changes in transcript levels versus the non-senescent group were calculated by the $2^{-\Delta\Delta C_t}$ method.

Luminex assay

The Luminex[®] Multiplex Assay Customization Tool (R&D Systems, Minneapolis, MN, USA) was used to generate an assay to detect analytes GDF15, MMP3, CXCL8/IL8, CCL5/RANTES, CXCL5/ENA78, CCL20/MIP3 α and CX3CL1/fractalkine, Luminex assay was performed as per manufacturer instructions. All incubations in this assay were performed at room temperature, on an orbital shaker at 800 rpm. Briefly, 50 μ L of the conditioned media or provided standard was loaded in each respective well along with 50 μ L of the provided microparticle cocktails. The plate was sealed and incubated, and then washed with the provided 1X wash buffer four times using a magnetic base below the plate. Subsequently, the wells were incubated with biotin and streptavidin, with washes after each step. After a final wash, the microparticles were resuspended in 100 μ L of 1X wash buffer, placed on the shaker for 2 minutes, and then read on the *FLEXMAP 3D*[®] provided by the Immune Monitoring Core of Fred Hutchinson Cancer Center Shared Resources. A 5-PL curve fit was used to plot standard graphs and analyte values were provided in pg/mL. After normalization to the corresponding cell count during media collection, fold changes in analytes compared to the NS group were calculated.

Biostatistical analyses

GraphPad Prism 7 software (GraphPad) was used to analyze the qPCR and Luminex data to determine statistical significance. Data were expressed as the mean \pm SEM. One way ANOVA was used to compare differences between groups in all experiments. $p \leq 0.05$ was considered as significant.

RESULTS

Senescence induction and confirmation

We established 7 lines of primary human colon fibroblasts from resected normal healthy rectosigmoid

colon from subjects with concurrent colon cancer. To induce senescence using genotoxic and oxidative stressors, we selected three different agents: doxorubicin, bleomycin and hydrogen peroxide as they induce senescence through different mechanisms: DNA alkylation and double-strand breakage; thymidine incorporation inhibition and single and double-strand DNA breakage; and oxidative stress, respectively. In addition, it is well known that the human colon mucosa is subject to exposure to alkylating and methylating agents and to oxidative stress making these agents physiologically relevant [37, 38]. A schematic representation of the overall study plan is described in Figure 1A. Following recovery for around 10 days from treatment initiation, cells displayed classic senescence features including flattened and enlarged morphology. Positive senescence associated Beta-galactosidase (SA- β -gal) activity at pH 6 (Figure 1B) was confirmed in more than 70% of the treated cells (Figure 1C) versus non-treated, proliferating control cell (hereon referred to as non-senescent (NS) controls).

Differentially expressed senescent transcriptomes

RNAseq analysis was performed on three patient-derived fibroblast lines using the HiSeq platform. Transcripts were analyzed for differential expression in senescent cells versus proliferating control cells using stringent criteria (FDR ≤ 0.01 and $\log_2(\text{fold change compared to NS}) \geq$ or ≤ 1). Out of 15,569 detected transcripts, several differentially regulated transcripts associated with inducer-specific senescence were found: 1538 transcripts in hydrogen peroxide-induced samples, 1492 in doxorubicin-induced samples, and 780 in bleomycin-induced samples. (Figure 2A). A Venn diagram (Figure 2B) was used to identify senescence-associated genes common to all methods of induction and is here-on referred to as the 'core senescent profile'. The complete list of differentially expressed genes in the core senescent profile is provided in Supplementary Table 2. As a secondary confirmation of senescence, we assessed the expression of known markers of senescence and identified elevated *CDKN1A/p21^{Cip1}* and *CDKN2A/p16^{Ink4a}*, and decreased *LMNB1* transcripts levels compared to the NS group (Supplementary Figure 1). Since the intent of the study was to identify genes that may contribute to the colon SASP, our further analyses focused on transcripts that are up-regulated with senescence.

Overall, the core senescent profile was composed of several upregulated cytokines and chemokines (*CXCL1/GRO α* , *CXCL2/GRO β* , *CXCL5/ENA78*, *CXCL8/IL8*, *CXCL14*, and *CCL2/MCP-1*, *CCL5/RANTES*, *CCL20/MIP3 α*), growth factors (*GDF15*, *BMP2*), proteases (*MMP3*, *MMP12*, *PLAT*,

SERPIN1), protease inhibitors (*CST1*, *CST2*, *CST4*, *C3*, *IGFBP2*), tumor necrosis factor receptors (*TNFSF13B*, *TNFRSF10C*), transmembrane proteins including transporters and channels, histones, signaling molecules (*NOTCH3*, *NR4A2*, *FOSC*, *RELB*, *STAT*), and glycoproteins such as *STC1*. We specifically assessed colon fibroblast senescence genes that could contribute to a SASP, modulate the tissue microenvironment, alter the function of the colon and potentially alter the risk for disease. We thus focused our validation studies on those transcripts that are translated to secreted proteins and focused on the core senescent profile shared by all the inducing agents, which interestingly, is enriched for secreted proteins ($p < 0.0001$). We selected eight candidates (*CST4*, *CCL20*, *CX3CL1*, *CXCL5*, *CXCL8*, *GDF15*, *CCL5* and *MMP3*) that play an important role in cancer pathogenesis for further study [3, 4, 8–12, 15, 39]. Another relevant SASP gene, *GDF15* has already been characterized for its pro-tumorigenic effects in CRC by our group [12]. We first performed RT-qPCR using transcript-specific pre-designed primer pairs to confirm the RNA-Seq results (Figure 2C). Expression levels of all transcripts were up-regulated in all senescent cells, except for *CX3CL1* and *CCL20*, which were below the detectable range in all samples. Conditioned media was then collected at the end of senescence induction to assess protein secretion

(Figure 3). After normalization to the number of cells contributing to the conditioned media, we confirmed the elevated secretion of *CXCL8*, *CCL20*, *CXCL5*, *GDF15*, *MMP3* and *CCL5* in senescent cells, while *CX3CL1* (fractalkine) was undetectable. Together, these findings confirm that elevated expression of *CXCL8*, *CCL20*, *CXCL5*, *GDF15*, *MMP3* and *CCL5* at the transcript and protein levels are part of a universal senescent colon fibroblast SASP.

Analyses of differentially regulated pathways and gene ontologies of the colon fibroblast core senescent profile

To further investigate a shift in cellular function corresponding to the senescent associated transcriptome, we scrutinized pathways upregulated by either doxorubicin, bleomycin or H_2O_2 -induced senescence as well as in the core senescent profile. We performed KEGG analysis for pathways enriched in stimulus-specific senescent transcriptomes as well as in the core senescent profile. The most robustly enriched pathways (Figure 4A) included the cytokine-cytokine receptor pathway and chemokine signaling pathways (list of genes in Supplementary Table 3). An enrichment of TNF pathway and NF- κ B signaling pathway was found, consistent with prior studies [40]. Analyses were

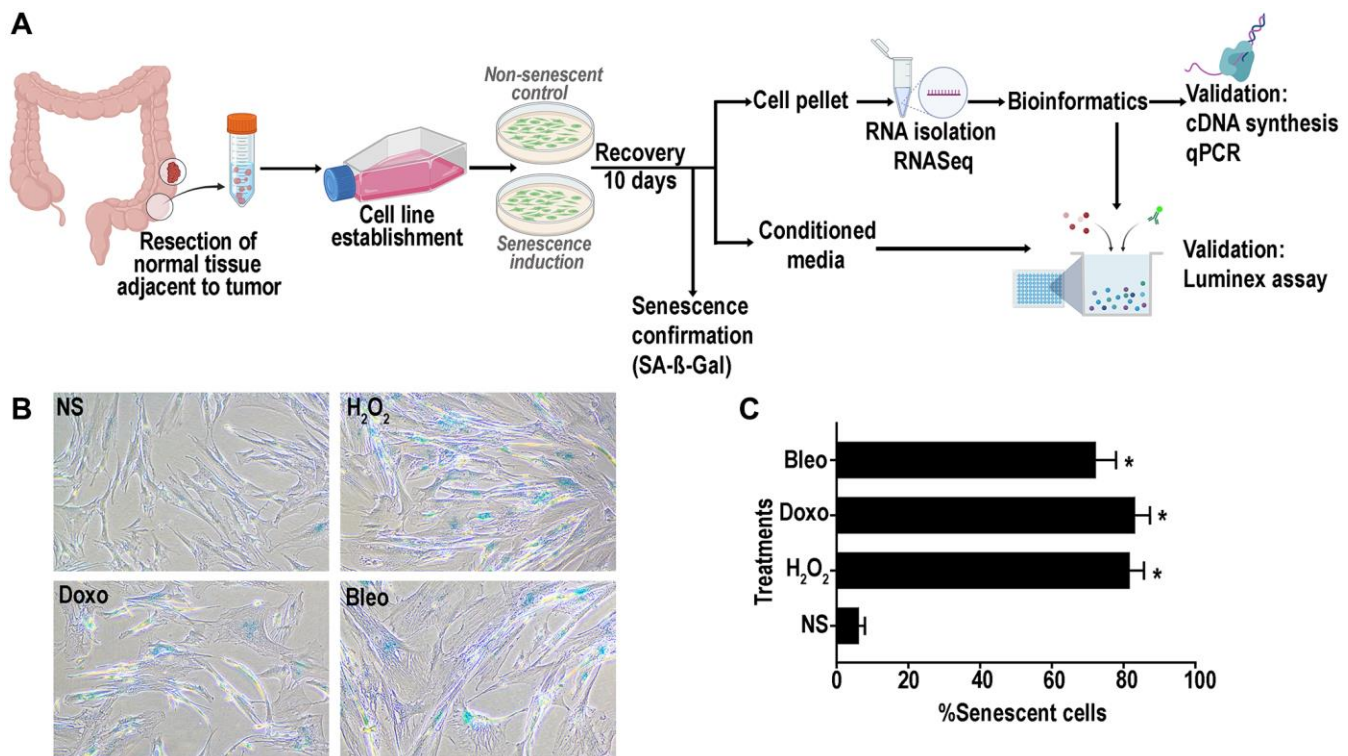


Figure 1. (A) Schematic representation of experimental design of senescence induction in the colon fibroblasts. Senescence was induced using hydrogen peroxide (H_2O_2 , 400 μ M), doxorubicin (doxo, 250 nM) or bleomycin (bleo, 10 ng/mL). Non-senescent proliferating (NS) cells were used as a control. (B) Representative SA- β -gal assay results at pH6 to confirm senescence induction in >70% of the cells. (C) Quantification of SA- β -gal positive senescent cells. (data are Mean \pm SEM * $p < 0.01$ versus NS).

also performed for gene ontology based on biological processes (GOBP) and molecular functions (GOMF) of the core senescence-associated profiles, which characterized the dominant biological processes and molecular functions of cells expressing this profile. We identified 25 top pathways (Figure 4B), which were selected after accounting for redundancies by collating all relevant pathways with over 90% gene overlap (full dataset in Supplementary Table 4A, 4B). Similar to KEGG analysis, GOBP identified several cytokine-

related biological processes with autocrine/paracrine significance including chemokine-mediated signaling pathway, cellular response to chemokine, and immune modulation including chemotaxis and migration of various immune cells (granulocytes, neutrophils, leukocytes and myeloid derived leukocytes). The core senescent profile also displayed the activation of several signal transduction cascades including STAT pathways (via tyrosine phosphorylation), MAPK and ERK pathways, calcium-mediated signaling

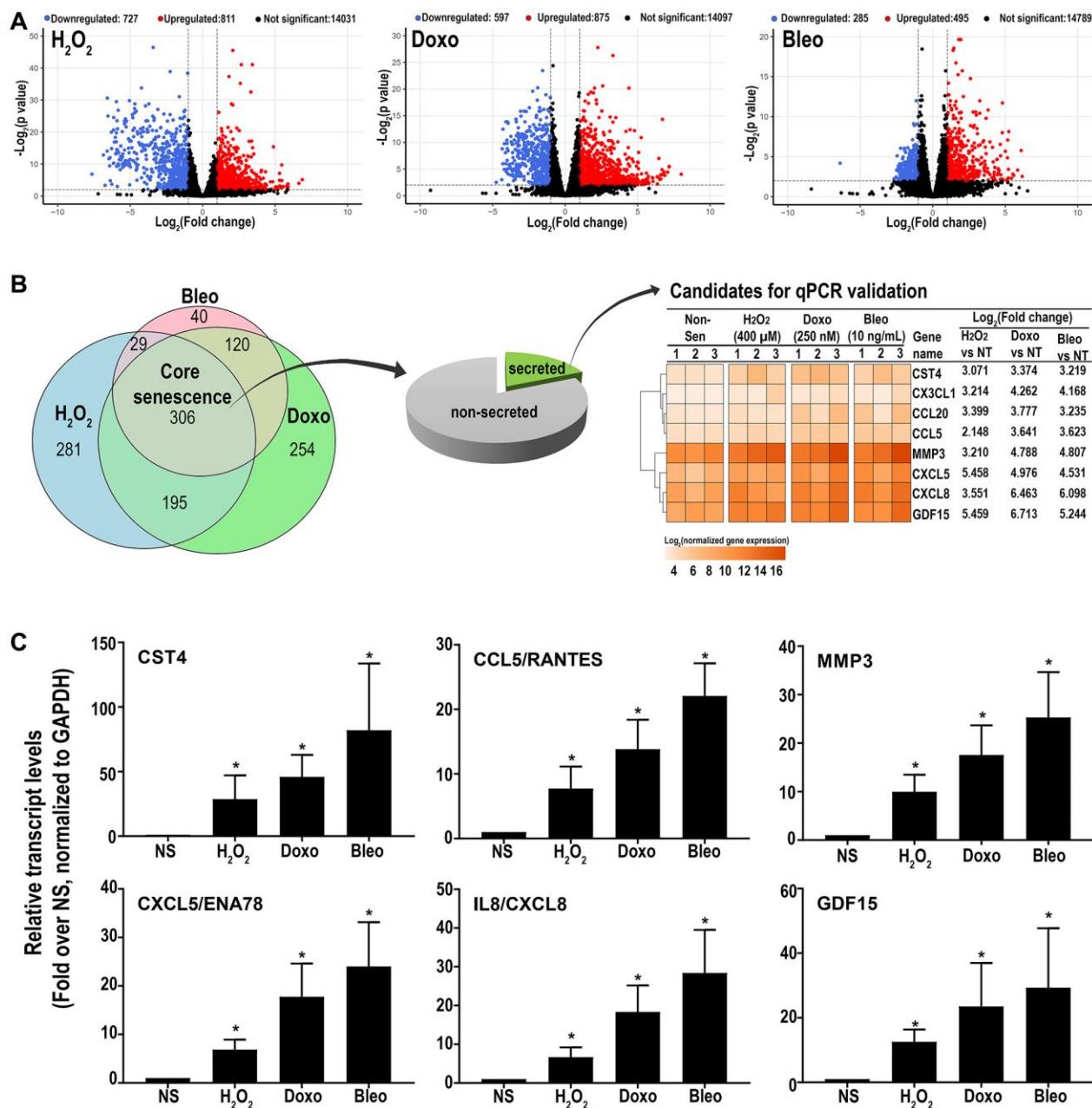


Figure 2. (A) Volcano plots of differentially expressed transcripts versus non-senescent proliferating (NS) cells (B) A Venn diagram showing a 'core senescent profile' of transcripts upregulated by all senescence inducers and heatmap of the eight candidates selected for validation at the transcriptomic level by qPCR (C). Data are Mean ± SEM (**p* < 0.04 versus NS) senescent or non-senescent fibroblast lines from 7 subjects. (C) Quantitative RT-PCR assay results of 6 genes in the core senescence SASP demonstrates increased expression of all of the genes by any of the senescence inducing agents.

pathway and G protein signaling pathways. The enrichment of transporter and channel activity, and calcium-ion regulatory mechanisms was also observed, indicating ionic flux in senescent cells. Analyses of molecular function (Figure 4C, Supplementary Table 5) similarly indicated the enrichment of chemokine-related activity, particularly that of CXCL8/IL8, inflammatory mechanisms, elevated activity of various transmembrane channels, activation of receptors to chemokines/cytokines and enzyme lytic activity, indicating an ability to modulate the surrounding milieu. Thus, KEGG, GOBP and GOMF together confirm a persistent elevation in cytokines and chemokines that

may have paracrine and systemic effects on the tissue microenvironment. Interestingly, our analyses did not identify any notable differences in pathways or GO's related to cancer or aging between the various treatments for senescence induction.

DISCUSSION

The role of senescence in pathophysiology has been well documented, as has the vast heterogeneity in the senescent profile across cell types [21–26]. Several senescence databases have been created including Cellular Senescence Network (SenNet), SenQuest by

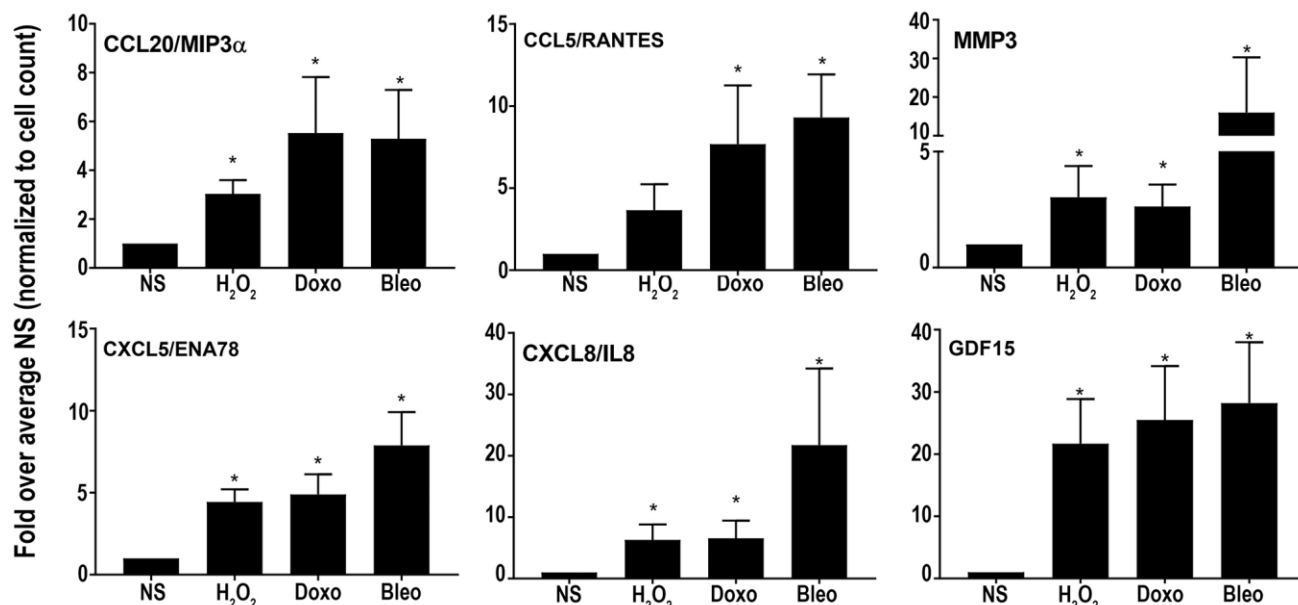


Figure 3. Levels of secreted SASP candidates in the conditioned media of senescent or non-senescent fibroblast lines from at least 6 subjects. All analytes were normalized to the cell count obtained during conditioned media collection and fold changes were calculated over respective NS group. Data are represented as Mean \pm SEM (* p < 0.05 versus NS). Abbreviation: NS: nonsenescent.

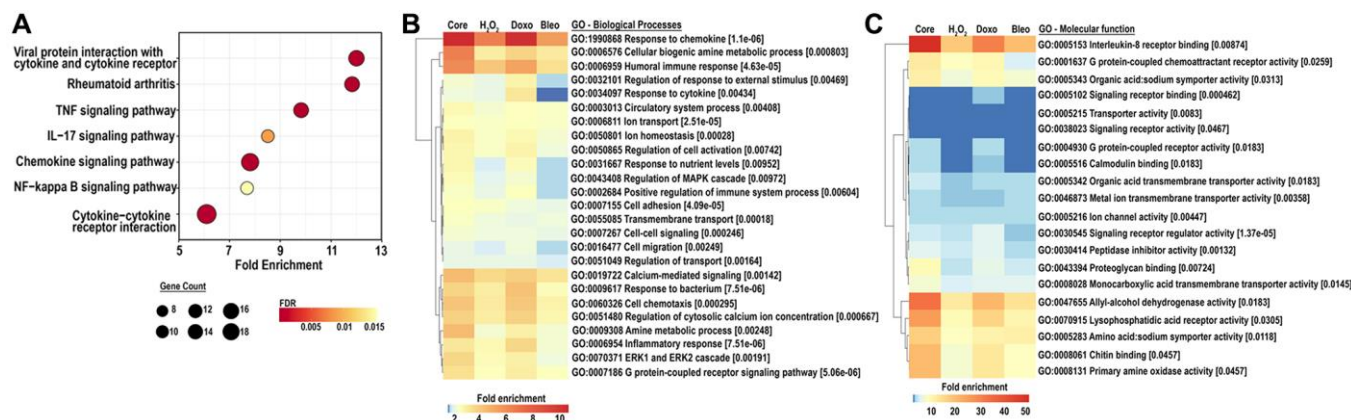


Figure 4. (A) KEGG analysis for the top 25 most enriched pathways in the core senescent profile (FDR \leq 0.01). Gene counts represent the number of differentially expressed genes, color scales represent the FDR, and fold enrichment is plotted on the x-axis. (B, C) GO analyses for biological processes and molecular function enriched in the colon fibroblast core senescent profile (FDR < 0.01). The top 25 entries are represented after removing redundant processes and functions.

the International Cell Senescence Association, CellAge [41] at the Human Ageing Genomic Resources, and the SASPAtlas [21]. While these databases serve as excellent resources to explore senescent phenotypes across multiple cell types, human colon fibroblasts have not been described in any of them. Our study fills in this knowledge gap by describing the senescent phenotype of primary human colon fibroblasts. Our study is of particular value because it informs our understanding of senescence in colon health and disease and the impact of secreted senescence products on shaping the tissue microenvironment in the colon. Using RNASeq, we generated an atlas of the senescent associated secretory phenotype of human colon fibroblasts after treatment with different classes of physiologically relevant senescence inducers and identified a core SASP profile that is shared by all the inducers. We used primary adult colon fibroblast lines to generate senescence profiles that are most likely to reflect the SASP of human *in vivo* fibroblasts. For a subset of the SASP genes, we confirmed that the senescence-associated transcripts do ultimately result in secreted proteins. We also identified key pathways and biological processes that are differentially regulated in colon fibroblast senescence through KEGG and GOBP/GOMF analysis.

Of interest, we identified a set of SASP proteins secreted by colon fibroblasts that are biologically plausible factors for affecting the health and disease of the colon in people. Notably, these SASP proteins include GDF15, CXCL5, CXCL8/IL8, CCL5/RANTES, and MMP3. Their impact in causing aging-associated changes such as inflammation, aging-related pathologies and in cancer mechanisms have also been previously demonstrated in mouse models and cell line systems. GDF15, a distant member of the transforming growth factor (TGF)- β superfamily, was initially recognized as macrophage inhibitory cytokine-1 (MIC-1) and noted for its ability to suppress various immune cells including other macrophages, dendritic cells, neutrophils, T cells and natural killer cells [42]. More recently, the plasma GDF15 level has been associated with age and is predictive of mortality and multimorbidity [43]. It signals via the GFRAL receptor [44] and has been shown to promote cancer hallmark behaviors in colon adenocarcinoma cells [12]. GDF15 is also a highly expressed SASP component in senescent dermal and pulmonary fibroblast and some epithelial lines that have been induced into senescence by a variety of methods [21–23].

It is notable that our core senescent profile includes chemokines of the CXCL- and CCL- families, including CXCL1, CXCL2, CXCL5, CXCL8, CXCL14, CCL2, and CCL20, have similarly been identified as SASP components in our studies and in previously published

studies [15, 26]. CXCL8/IL8 is a well-studied chemokine in multiple cancer types, including colorectal, esophageal, bladder, gastric, breast, and others [45]. CXCL8 acts as a strong chemoattractant, potentially increasing tumor-promoting behaviors including tumor proliferation, migration, invasion, anoikis suppression, an epithelial to mesenchymal transition (EMT) [39, 46–49]. CXCL8 can also suppress immune responses in the surrounding microenvironment [45, 50, 51]. Recent evidence suggests that increasing serum CXCL8 levels can predict resistance to anti-PD-1 immunotherapy in non-small-cell lung cancer patients, which has led to the development of targeted therapies directed at CXCL8 (e.g., HuMax-IL8) for the treatment of some types of cancers [52, 53]. Besides its role in cancer, CXCL8, along with CXCL1, 2, and 5 are noted for their autocrine and/or paracrine effects in reinforcing senescence. This occurs when these chemokines bind the CXCR2 receptor which leads to the downstream activations of the NF- κ B signaling pathway [54]. CCL20 has similarly also been noted for reinforcing a senescence phenotype [4, 55]. Of note, these SASP cytokines can further propagate senescence in neighboring cells, thus shaping a broader senescent tissue microenvironment [4, 55, 56].

In addition to GDF15 and the chemokines and cytokines we observed in the colon fibroblast SASP, we also identified several other SASP proteins that may mediate health and disease in the colon *in vivo*. Matrix metalloproteinases 3 and 12 (MMP3 and 12), which are elevated in the colon core senescent phenotype, have also been also reported in previously described senescent cell line studies and are robustly elevated in senescent murine tissue [57, 58]. Interestingly, the elevation of several well-reported [15] senescence-induced targets including *IL1A*, *IL1B*, *IL33*, and *IL6* was observed to be senescence inducer specific in colon cells and thus were excluded from the core senescent profile, reflecting the heterogeneity in senescence that results from different etiologies.

Our KEGG and GO analyses highlighted the cytokine and chemokine mediated events, including the TNF pathway and NF- κ B signaling pathway. Besides being amplified by autocrine effects of cytokines, the TNF and NF- κ B pathways have also been frequently associated with senescence and aging [40]. In the colon fibroblasts, the senescence associated NF- κ B pathway appeared to be driven through the canonical mechanism (involving *cIAP1/2* or *BIRC2*, *CXCL8* and *VCAM1*) as well as non-canonical mechanisms (involving *BAFF*, *CD40*, and *RELB*) (Supplemental Table 3). Germane to our findings, senomorphic therapies that prevent the production of the SASP, may do so by inhibiting the NF- κ B pathway directly (e.g.,

resveratrol, metformin, etc.) or indirectly through mTOR inhibition (e.g., rapamycin). These agents are under investigation for their ability to minimize or prevent age-related and chronic pathologies [59]. Interestingly we also observed an enrichment of pathways associated with rheumatoid arthritis and atherosclerosis, both of which are age-associated and inflammatory diseases. GOBP and GOMF analyses of the SASP subset of the core senescent profile are suggestive of paracrine processes include extracellular matrix disassembly, organization, extracellular structure organization and collagen catabolic process (Supplementary Table 6A, 6B). Indeed, these observations support the hypothesis that senescent cell accumulation secondary to increased oxidative stress, exposure to DNA alkylating agents, or age can create an environment with persistent elevation in pro-inflammatory cytokines and chemokines, that can eventually lead to modulation of the surrounding matrix and chronic activation of inflammatory processes [3, 4, 8, 10, 11, 15, 60].

It is notable that our results have similarities to a variety of other senescent associated datasets. Firstly, we compared colon fibroblast senescence transcriptome to a human aging secretome [61]. We found that *GDF15*, *CXCL1*, *CXCL8*, *CXCL14*, *CCL5*, and several other core senescence candidates (Supplementary Table 7), overlap with aging-related secretome, as previously described. We next assessed commonalities of the colon fibroblast senescent phenotype with previously described phenotypes of senescent fibroblasts in tissues other than the colon. We focused on a large proteomic study and meta-analysis on the SASP of pulmonary fibroblasts induced into senescence by irradiation, oncogene activation and atazanavir treatment [21]. The genes upregulated in all three conditions that overlapped the colon core senescence included *AKR1B1*, *IGFBP2*, *C3*, *CXCL1*, *STC1* and *GDF15* (FDR <0.01). Of these, *GDF15* was consistently upregulated in a ‘universal senescent profile’ of various epithelial and fibroblast cell lines. We also found that doxorubicin-induced-senescence of pulmonary fibroblasts [22] shared 61% of the colon doxorubicin-induced transcripts, including the validated core colon senescence candidates *CCL20*, *CXCL5*, *CST4*, *GDF15*, *MMP3*, as well as other targets including *AKR1B1*, *IGFBP2*, *C3*, *CXCL1*, and *STC1*. Lastly, we compared our results with those in the SenMayo gene set, a physiologically relevant senescence gene set [26], which is curated to accurately identify senescent cells with aging across tissues and species. We found that that nearly a quarter of the SenMayo list overlaps with the core senescent colon fibroblast profile, and of these, four genes (*GDF15*, *CXCL1*, *C3* and *IGFBP2*) are also common

to the Basisty universal fibroblast senescent signature [21]. In aggregate, our observations support the concept that senescence-associated profiles have several commonalities among cell types but are also very heterogenous and specific to cell type and method of induction.

We similarly compared the phenotype of senescent human colon fibroblasts to that of cancer-associated fibroblasts (CAFs), which occur in the immediate tumor microenvironment. Similar to senescent fibroblasts, CAFs are large in size and have indented nuclei. They secrete a variety of growth factors, chemokines, extracellular matrix (ECM) proteins and well as ECM-degrading metalloproteases, which have been implicated in promoting oncogenic behaviors of cancer and in resistance to anti-cancer therapies [62–69]. Evidence also supports a role for senescent CAFs in tumor progression [70–72]. Overall, a large similarity has been observed in oncogenic secretions from CAFs and senescent non-cancer cells. Single cell sequencing has shown that CAFs are heterogenous in origin and can be functionally categorized as inflammatory, complement presenting, myofibroblastic and antigen presenting [63, 73–77]. Specifically relevant to the CRC microenvironment and senescence are the subsets of CAF subsets described by Pelka et al. (2021) that exhibited elevated levels of an inflammatory program, including genes *MMP1*, *MMP3*, *CXCL8* and *CXCL1*, which are colon fibroblast SASP components observed in our study. Additional SASP components observed in our studies (*CXCL14*, *BMP4*, *HSD17B2*, *CCL13*, *TCF21*, *SOD2*, and *F3*) formed the characterizing features of various other CAF subsets in this same study [74]. Thus, similar to CAFs, human colon fibroblast SASP can be speculated to have a variety of roles in modulating the surrounding niche in colon pathophysiology and perhaps inducing oncogenic effects in the colon.

Finally, we wish to note that although our studies have many strengths, they also have limitations. These limitations include a significant degree of subject-based heterogeneity in senescence within the same cell type that is independent of the senescence-induction regimen used, assessment of the SASP at only one time point after induction by the senescence inducing agent, and no assessment of single cell responses to the SASP inducing agent.

In conclusion, we have defined a core senescent transcriptome and SASP for primary human colon fibroblasts, validated a subset of important SASP associated secreted proteins, and described noteworthy SASP mediated changes in pathways, biological

processes, and molecular functions. Based on our analyses, we propose that elevated expression *GDF15*, *MMP3*, *CXCL8*, *CXCL1*, *CXCL5*, *STC1* and *CCL5* are a core set of SASP genes of senescent colon and non-colon fibroblasts, which may be of use for identifying senescent cells in tissues. Our studies have also helped inform the candidate driver proteins involved in senescence-associated diseases like CRC. These candidates might also prove worthy targets for anti-senescence therapies, which is a class of therapy currently under investigation for the prevention of age-related disease in people. Further studies will be needed to address the limitations of our study and to translate our understanding of the SASP and disease into clinical care.

Abbreviations

SASP: Senescence associated secretory phenotype; CXCL-1,-2,-5,-8 and -14: C-X-C motif chemokine ligand 1, 2, 5, 8, and 14, respectively; MMP3 or MMP12: matrix metalloproteinase 3 and 12 respectively; CCL2, 5 and 20: C-C motif chemokine ligand 2, 5, and 20 respectively; CX3CL1: C-X3-C motif chemokine ligand 1; GDF15: growth differentiation factor 15; BMP2: bone morphogenetic protein 2; PLAT: plasminogen activator, tissue type; SERPINI1: serpin family I member 1; CST1: cystatin SN; CST 2: cystatin SA ; CST4: cystatin S; C3: complement C3; IGFBP2: insulin like growth factor binding protein 2; TNF: tumor necrosis factor; TNFSF13B/BAFF: TNF superfamily member 13b; TNFRSF10C: TNF receptor superfamily member 10c; NF- κ B: nuclear factor kappa B; NOTCH3: notch receptor 3; NR4A2: nuclear receptor subfamily 4 group A member 2; FOSB: FosB proto-oncogene, AP-1 transcription factor subunit; RELB: RELB proto-oncogene, NF- κ B subunit; STAT1: signal transducer and activator of transcription 1; STC1: stanniocalcin 1; cIAP1/2: Cellular Inhibitor of Apoptosis Protein 1/2; BIRC2: baculoviral IAP repeat containing 2; VCAM1: vascular cell adhesion molecule 1; CD40: CD40 molecule; RELB: RELB proto-oncogene, NF- κ B subunit; KEGG: Kyoto Encyclopedia of Genes and Genomes.

AUTHOR CONTRIBUTIONS

N.H., M.Y., and W.M.G. conceived the study and experiments, N.H. and K.C. performed the experiments, N.H. analyzed the data; T.W. and B.M.R. performed bioinformatics analyses under the supervision of N.H. and M.Y., J.L.A. collected the procured tissue used in the study, N.H. wrote the original draft of the manuscript, M.Y. and W.M.G. reviewed and revised the manuscript; all authors reviewed the manuscript prior to submission.

ACKNOWLEDGMENTS

We would like to thank the ColoCare study team for their efforts towards subject recruitment.

CONFLICTS OF INTEREST

W. M. Grady is a scientific advisory board member for Freenome, Guardant Health, and SEngine and consultant for DiaCarta, Natera, Guidepoint and GLG. He receives research support from LucidDx.

ETHICAL STATEMENT AND CONSENT

All studies in this manuscript were reviewed and approved by the Cancer Consortium (Fred Hutchinson Cancer Center, and University of Washington School of Medicine) IRB Committee. The protocol approval number is STUDY00002161. The specimens were obtained after the informed consent of participants.

FUNDING

This research was supported by National Cancer Institute (NCI), Inter-disciplinary Training Grant in Cancer T32 CA080416 to NGH; National Institutes of Health, Grant/Award Number: P30CA15704, UO1CA152756, RO1CA220004, U54CA274374, UO1AG077920, U2CCA271902; Listwin Family Foundation; Cottrell Family Fund; R.A.C.E. Charities; Seattle Translational Tumor Research; Rodger C. Haggitt Endowed Chair; W.H. Geiger Family Foundation to WMG; National Cancer Institute, Grant/Award Number: R50CA233042 to MY.

REFERENCES

1. Kuipers EJ, Grady WM, Lieberman D, Seufferlein T, Sung JJ, Boelens PG, van de Velde CJ, Watanabe T. Colorectal cancer. *Nat Rev Dis Primers*. 2015; 1:15065. <https://doi.org/10.1038/nrdp.2015.65> PMID:[27189416](https://pubmed.ncbi.nlm.nih.gov/27189416/)
2. Hayflick L, Moorhead PS. The serial cultivation of human diploid cell strains. *Exp Cell Res*. 1961; 25:585–621. [https://doi.org/10.1016/0014-4827\(61\)90192-6](https://doi.org/10.1016/0014-4827(61)90192-6) PMID:[13905658](https://pubmed.ncbi.nlm.nih.gov/13905658/)
3. Campisi J. Aging, cellular senescence, and cancer. *Annu Rev Physiol*. 2013; 75:685–705. <https://doi.org/10.1146/annurev-physiol-030212-183653> PMID:[23140366](https://pubmed.ncbi.nlm.nih.gov/23140366/)
4. Paramos-de-Carvalho D, Jacinto A, Saúde L. The right

- time for senescence. *Elife*. 2021; 10:e72449.
<https://doi.org/10.7554/eLife.72449>
PMID:[34756162](https://pubmed.ncbi.nlm.nih.gov/34756162/)
5. Pignolo RJ, Passos JF, Khosla S, Tchkonja T, Kirkland JL. Reducing Senescent Cell Burden in Aging and Disease. *Trends Mol Med*. 2020; 26:630–8.
<https://doi.org/10.1016/j.molmed.2020.03.005>
PMID:[32589933](https://pubmed.ncbi.nlm.nih.gov/32589933/)
 6. Coppé JP, Patil CK, Rodier F, Sun Y, Muñoz DP, Goldstein J, Nelson PS, Desprez PY, Campisi J. Senescence-associated secretory phenotypes reveal cell-nonautonomous functions of oncogenic RAS and the p53 tumor suppressor. *PLoS Biol*. 2008; 6:2853–68.
<https://doi.org/10.1371/journal.pbio.0060301>
PMID:[19053174](https://pubmed.ncbi.nlm.nih.gov/19053174/)
 7. Adams PD. Healing and hurting: molecular mechanisms, functions, and pathologies of cellular senescence. *Mol Cell*. 2009; 36:2–14.
<https://doi.org/10.1016/j.molcel.2009.09.021>
PMID:[19818705](https://pubmed.ncbi.nlm.nih.gov/19818705/)
 8. Childs BG, Durik M, Baker DJ, van Deursen JM. Cellular senescence in aging and age-related disease: from mechanisms to therapy. *Nat Med*. 2015; 21:1424–35.
<https://doi.org/10.1038/nm.4000>
PMID:[26646499](https://pubmed.ncbi.nlm.nih.gov/26646499/)
 9. Demaria M, Ohtani N, Youssef SA, Rodier F, Toussaint W, Mitchell JR, Laberge RM, Vijg J, Van Steeg H, Dollé ME, Hoeijmakers JH, de Bruin A, Hara E, Campisi J. An essential role for senescent cells in optimal wound healing through secretion of PDGF-AA. *Dev Cell*. 2014; 31:722–33.
<https://doi.org/10.1016/j.devcel.2014.11.012>
PMID:[25499914](https://pubmed.ncbi.nlm.nih.gov/25499914/)
 10. Muñoz-Espín D, Serrano M. Cellular senescence: from physiology to pathology. *Nat Rev Mol Cell Biol*. 2014; 15:482–96.
<https://doi.org/10.1038/nrm3823>
PMID:[24954210](https://pubmed.ncbi.nlm.nih.gov/24954210/)
 11. Kuilman T, Peeper DS. Senescence-messaging secretome: SMS-ing cellular stress. *Nat Rev Cancer*. 2009; 9:81–94.
<https://doi.org/10.1038/nrc2560>
PMID:[19132009](https://pubmed.ncbi.nlm.nih.gov/19132009/)
 12. Guo Y, Ayers JL, Carter KT, Wang T, Maden SK, Edmond D, Newcomb P P, Li C, Ulrich C, Yu M, Grady WM. Senescence-associated tissue microenvironment promotes colon cancer formation through the secretory factor GDF15. *Aging Cell*. 2019; 18:e13013.
<https://doi.org/10.1111/acer.13013>
PMID:[31389184](https://pubmed.ncbi.nlm.nih.gov/31389184/)
 13. Krishnamurthy J, Torrice C, Ramsey MR, Kovalev GI, Al-Regaiey K, Su L, Sharpless NE. Ink4a/Arf expression is a biomarker of aging. *J Clin Invest*. 2004; 114:1299–307.
<https://doi.org/10.1172/JCI22475>
PMID:[15520862](https://pubmed.ncbi.nlm.nih.gov/15520862/)
 14. Ressler S, Bartkova J, Niederegger H, Bartek J, Scharffetter-Kochanek K, Jansen-Dürr P, Wlaschek M. p16INK4A is a robust in vivo biomarker of cellular aging in human skin. *Aging Cell*. 2006; 5:379–89.
<https://doi.org/10.1111/j.1474-9726.2006.00231.x>
PMID:[16911562](https://pubmed.ncbi.nlm.nih.gov/16911562/)
 15. Coppé JP, Desprez PY, Krtolica A, Campisi J. The senescence-associated secretory phenotype: the dark side of tumor suppression. *Annu Rev Pathol*. 2010; 5:99–118.
<https://doi.org/10.1146/annurev-pathol-121808-102144>
PMID:[20078217](https://pubmed.ncbi.nlm.nih.gov/20078217/)
 16. Krtolica A, Parrinello S, Lockett S, Desprez PY, Campisi J. Senescent fibroblasts promote epithelial cell growth and tumorigenesis: a link between cancer and aging. *Proc Natl Acad Sci U S A*. 2001; 98:12072–7.
<https://doi.org/10.1073/pnas.211053698>
PMID:[11593017](https://pubmed.ncbi.nlm.nih.gov/11593017/)
 17. Dimri GP, Lee X, Basile G, Acosta M, Scott G, Roskelley C, Medrano EE, Linskens M, Rubelj I, Pereira-Smith O. A biomarker that identifies senescent human cells in culture and in aging skin in vivo. *Proc Natl Acad Sci U S A*. 1995; 92:9363–7.
<https://doi.org/10.1073/pnas.92.20.9363>
PMID:[7568133](https://pubmed.ncbi.nlm.nih.gov/7568133/)
 18. Baker DJ, Wijshake T, Tchkonja T, LeBrasseur NK, Childs BG, van de Sluis B, Kirkland JL, van Deursen JM. Clearance of p16^{INK4a}-positive senescent cells delays ageing-associated disorders. *Nature*. 2011; 479:232–6.
<https://doi.org/10.1038/nature10600>
PMID:[22048312](https://pubmed.ncbi.nlm.nih.gov/22048312/)
 19. Patil P, Dong Q, Wang D, Chang J, Wiley C, Demaria M, Lee J, Kang J, Niedernhofer LJ, Robbins PD, Sowa G, Campisi J, Zhou D, Vo N. Systemic clearance of p16^{INK4a}-positive senescent cells mitigates age-associated intervertebral disc degeneration. *Aging Cell*. 2019; 18:e12927.
<https://doi.org/10.1111/acer.12927>
PMID:[30900385](https://pubmed.ncbi.nlm.nih.gov/30900385/)
 20. Ogrodnik M, Evans SA, Fielder E, Victorelli S, Kruger P, Salmonowicz H, Weigand BM, Patel AD, Pirtskhalava T, Inman CL, Johnson KO, Dickinson SL, Rocha A, et al. Whole-body senescent cell clearance alleviates age-related brain inflammation and cognitive impairment in mice. *Aging Cell*. 2021; 20:e13296.
<https://doi.org/10.1111/acer.13296>
PMID:[33470505](https://pubmed.ncbi.nlm.nih.gov/33470505/)

21. Basisty N, Kale A, Jeon OH, Kuehnemann C, Payne T, Rao C, Holtz A, Shah S, Sharma V, Ferrucci L, Campisi J, Schilling B. A proteomic atlas of senescence-associated secretomes for aging biomarker development. *PLoS Biol.* 2020; 18:e3000599. <https://doi.org/10.1371/journal.pbio.3000599> PMID:[31945054](https://pubmed.ncbi.nlm.nih.gov/31945054/)
22. Casella G, Munk R, Kim KM, Piao Y, De S, Abdelmohsen K, Gorospe M. Transcriptome signature of cellular senescence. *Nucleic Acids Res.* 2019; 47:11476. <https://doi.org/10.1093/nar/gkz879> PMID:[31612919](https://pubmed.ncbi.nlm.nih.gov/31612919/)
23. Hernandez-Segura A, de Jong TV, Melov S, Guryev V, Campisi J, Demaria M. Unmasking Transcriptional Heterogeneity in Senescent Cells. *Curr Biol.* 2017; 27:2652–60.e4. <https://doi.org/10.1016/j.cub.2017.07.033> PMID:[28844647](https://pubmed.ncbi.nlm.nih.gov/28844647/)
24. Özcan S, Alessio N, Acar MB, Mert E, Omerli F, Peluso G, Galderisi U. Unbiased analysis of senescence associated secretory phenotype (SASP) to identify common components following different genotoxic stresses. *Aging (Albany NY).* 2016; 8:1316–29. <https://doi.org/10.18632/aging.100971> PMID:[27288264](https://pubmed.ncbi.nlm.nih.gov/27288264/)
25. Purcell M, Kruger A, Tainsky MA. Gene expression profiling of replicative and induced senescence. *Cell Cycle.* 2014; 13:3927–37. <https://doi.org/10.4161/15384101.2014.973327> PMID:[25483067](https://pubmed.ncbi.nlm.nih.gov/25483067/)
26. Saul D, Kosinsky RL, Atkinson EJ, Doolittle ML, Zhang X, LeBrasseur NK, Pignolo RJ, Robbins PD, Niedernhofer LJ, Ikeno Y, Jurk D, Passos JF, Hickson LJ, et al. A new gene set identifies senescent cells and predicts senescence-associated pathways across tissues. *Nat Commun.* 2022; 13:4827. <https://doi.org/10.1038/s41467-022-32552-1> PMID:[35974106](https://pubmed.ncbi.nlm.nih.gov/35974106/)
27. Crowe EP, Tuzer F, Gregory BD, Donahue G, Gosai SJ, Cohen J, Leung YY, Yetkin E, Nativio R, Wang LS, Sell C, Bonini NM, Berger SL, et al. Changes in the Transcriptome of Human Astrocytes Accompanying Oxidative Stress-Induced Senescence. *Front Aging Neurosci.* 2016; 8:208. <https://doi.org/10.3389/fnagi.2016.00208> PMID:[27630559](https://pubmed.ncbi.nlm.nih.gov/27630559/)
28. Marthandan S, Baumgart M, Priebe S, Groth M, Schaer J, Kaether C, Guthke R, Cellerino A, Platzer M, Diekmann S, Hemmerich P. Conserved Senescence Associated Genes and Pathways in Primary Human Fibroblasts Detected by RNA-Seq. *PLoS One.* 2016; 11:e0154531. <https://doi.org/10.1371/journal.pone.0154531> PMID:[27140416](https://pubmed.ncbi.nlm.nih.gov/27140416/)
29. Andrews S. FASTQC: A quality control tool for high throughput sequence data. 2010.
30. Krueger F, Galore T. A wrapper tool around Cutadapt and FastQC to consistently apply quality and adapter trimming to FastQ files. 2015.
31. Martin M. Cutadapt Removes Adapter Sequences From High-Throughput Sequencing Reads. *EMBnetjournal.* 2011; 17:10–2. <https://doi.org/10.14806/ej.17.1.200>
32. Dobin A, Davis CA, Schlesinger F, Drenkow J, Zaleski C, Jha S, Batut P, Chaisson M, Gingeras TR. STAR: ultrafast universal RNA-seq aligner. *Bioinformatics.* 2013; 29:15–21. <https://doi.org/10.1093/bioinformatics/bts635> PMID:[23104886](https://pubmed.ncbi.nlm.nih.gov/23104886/)
33. Li B, Dewey CN. RSEM: accurate transcript quantification from RNA-Seq data with or without a reference genome. *BMC Bioinformatics.* 2011; 12:323. <https://doi.org/10.1186/1471-2105-12-323> PMID:[21816040](https://pubmed.ncbi.nlm.nih.gov/21816040/)
34. Love MI, Huber W, Anders S. Moderated estimation of fold change and dispersion for RNA-seq data with DESeq2. *Genome Biol.* 2014; 15:550. <https://doi.org/10.1186/s13059-014-0550-8> PMID:[25516281](https://pubmed.ncbi.nlm.nih.gov/25516281/)
35. *Bioinformatics and Computational Biology Solutions Using R and Bioconductor.* Edited by Gentleman R, Carey VJ, Huber W, Irizarry RA, Dudoit S. In: *Statistics for Biology and Health.* Springer New York, NY. 2005. <https://doi.org/10.1007/0-387-29362-0>
36. Upton GJG. Fisher's Exact Test. *J R Stat Soc Ser A Stat Soc.* 1992; 155:395–402. <https://doi.org/10.2307/2982890>
37. Povey AC, Hall CN, Badawi AF, Cooper DP, O'Connor PJ. Elevated levels of the pro-carcinogenic adduct, O(6)-methylguanine, in normal DNA from the cancer prone regions of the large bowel. *Gut.* 2000; 47:362–5. <https://doi.org/10.1136/gut.47.3.362> PMID:[10940272](https://pubmed.ncbi.nlm.nih.gov/10940272/)
38. Wang YJ, Chen Y, Zhang X, Lu Y, Chen H. New insights in intestinal oxidative stress damage and the health intervention effects of nutrients: A review. *J Funct Foods.* 2020; 75:104248. <https://doi.org/10.1016/j.jff.2020.104248>
39. Guo Y, Zang Y, Lv L, Cai F, Qian T, Zhang G, Feng Q. IL-8 promotes proliferation and inhibition of apoptosis via STAT3/AKT/NF-κB pathway in prostate cancer. *Mol Med Rep.* 2017; 16:9035–42. <https://doi.org/10.3892/mmr.2017.7747>

PMID:[29039490](#)

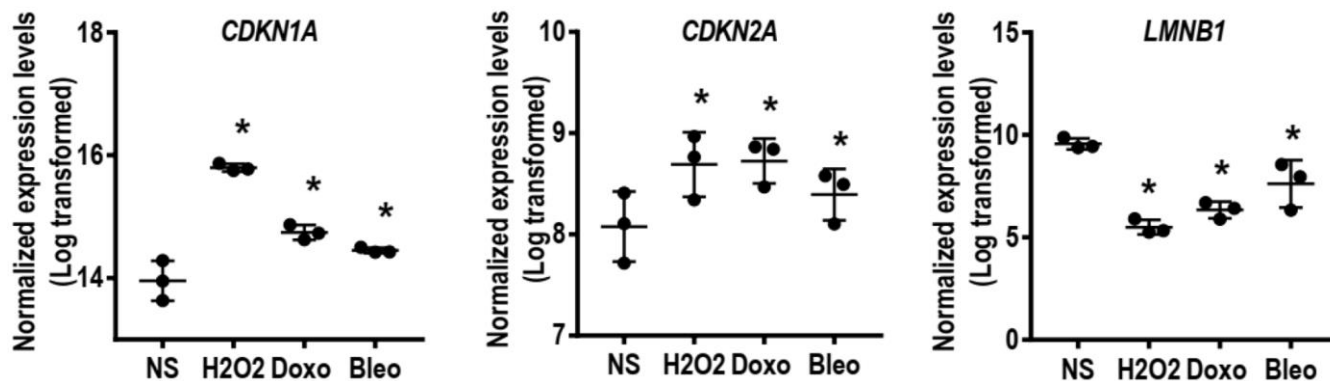
40. Salminen A, Kauppinen A, Kaarniranta K. Emerging role of NF- κ B signaling in the induction of senescence-associated secretory phenotype (SASP). *Cell Signal*. 2012; 24:835–45.
<https://doi.org/10.1016/j.cellsig.2011.12.006>
PMID:[22182507](#)
41. Avelar RA, Ortega JG, Tacutu R, Tyler EJ, Bennett D, Binetti P, Budovsky A, Chatsirisupachai K, Johnson E, Murray A, Shields S, Tejada-Martinez D, Thornton D, et al. A multidimensional systems biology analysis of cellular senescence in aging and disease. *Genome Biol*. 2020; 21:91.
<https://doi.org/10.1186/s13059-020-01990-9>
PMID:[32264951](#)
42. Schafer MJ, Zhang X, Kumar A, Atkinson EJ, Zhu Y, Jachim S, Mazula DL, Brown AK, Berning M, Aversa Z, Kotajarvi B, Bruce CJ, Greason KL, et al. The senescence-associated secretome as an indicator of age and medical risk. *JCI Insight*. 2020; 5:133668.
<https://doi.org/10.1172/jci.insight.133668>
PMID:[32554926](#)
43. Tanaka T, Basisty N, Fantoni G, Candia J, Moore AZ, Biancotto A, Schilling B, Bandinelli S, Ferrucci L. Plasma proteomic biomarker signature of age predicts health and life span. *Elife*. 2020; 9:e61073.
<https://doi.org/10.7554/eLife.61073>
PMID:[33210602](#)
44. Suriben R, Chen M, Higbee J, Oeffinger J, Ventura R, Li B, Mondal K, Gao Z, Ayupova D, Taskar P, Li D, Starck SR, Chen HH, et al. Antibody-mediated inhibition of GDF15-GFRAL activity reverses cancer cachexia in mice. *Nat Med*. 2020; 26:1264–70.
<https://doi.org/10.1038/s41591-020-0945-x>
PMID:[32661391](#)
45. Xiong X, Liao X, Qiu S, Xu H, Zhang S, Wang S, Ai J, Yang L. CXCL8 in Tumor Biology and Its Implications for Clinical Translation. *Front Mol Biosci*. 2022; 9:723846.
<https://doi.org/10.3389/fmolb.2022.723846>
PMID:[35372515](#)
46. Kumar S, O'Malley J, Chaudhary AK, Inigo JR, Yadav N, Kumar R, Chandra D. Hsp60 and IL-8 axis promotes apoptosis resistance in cancer. *Br J Cancer*. 2019; 121:934–43.
<https://doi.org/10.1038/s41416-019-0617-0>
PMID:[31673102](#)
47. Liu Q, Li A, Tian Y, Wu JD, Liu Y, Li T, Chen Y, Han X, Wu K. The CXCL8-CXCR1/2 pathways in cancer. *Cytokine Growth Factor Rev*. 2016; 31:61–71.
<https://doi.org/10.1016/j.cytogfr.2016.08.002>
PMID:[27578214](#)
48. David JM, Dominguez C, Hamilton DH, Palena C. The IL-8/IL-8R Axis: A Double Agent in Tumor Immune Resistance. *Vaccines (Basel)*. 2016; 4:22.
<https://doi.org/10.3390/vaccines4030022>
PMID:[27348007](#)
49. Long X, Ye Y, Zhang L, Liu P, Yu W, Wei F, Ren X, Yu J. IL-8, a novel messenger to cross-link inflammation and tumor EMT via autocrine and paracrine pathways (Review). *Int J Oncol*. 2016; 48:5–12.
<https://doi.org/10.3892/ijo.2015.3234>
PMID:[26548401](#)
50. Alfaro C, Sanmamed MF, Rodríguez-Ruiz ME, Teijeira Á, Oñate C, González Á, Ponz M, Schalper KA, Pérez-Gracia JL, Melero I. Interleukin-8 in cancer pathogenesis, treatment and follow-up. *Cancer Treat Rev*. 2017; 60:24–31.
<https://doi.org/10.1016/j.ctrv.2017.08.004>
PMID:[28866366](#)
51. Fousek K, Horn LA, Palena C. Interleukin-8: A chemokine at the intersection of cancer plasticity, angiogenesis, and immune suppression. *Pharmacol Ther*. 2021; 219:107692.
<https://doi.org/10.1016/j.pharmthera.2020.107692>
PMID:[32980444](#)
52. Bilusic M, Heery CR, Collins JM, Donahue RN, Palena C, Madan RA, Karzai F, Martí JL, Strauss J, Gatti-Mays ME, Schlom J, Gulley JL. Phase I trial of HuMax-IL8 (BMS-986253), an anti-IL-8 monoclonal antibody, in patients with metastatic or unresectable solid tumors. *J Immunother Cancer*. 2019; 7:240.
<https://doi.org/10.1186/s40425-019-0706-x>
PMID:[31488216](#)
53. Dominguez C, McCampbell KK, David JM, Palena C. Neutralization of IL-8 decreases tumor PMN-MDSCs and reduces mesenchymalization of claudin-low triple-negative breast cancer. *JCI Insight*. 2017; 2:94296.
<https://doi.org/10.1172/jci.insight.94296>
PMID:[29093275](#)
54. Acosta JC, O'Loughlen A, Banito A, Guijarro MV, Augert A, Raguz S, Fumagalli M, Da Costa M, Brown C, Popov N, Takatsu Y, Melamed J, d'Adda di Fagagna F, et al. Chemokine signaling via the CXCR2 receptor reinforces senescence. *Cell*. 2008; 133:1006–18.
<https://doi.org/10.1016/j.cell.2008.03.038>
PMID:[18555777](#)
55. Acosta JC, Banito A, Wuestefeld T, Georgilis A, Janich P, Morton JP, Athineos D, Kang TW, Lasitschka F, Andrulis M, Pascual G, Morris KJ, Khan S, et al. A complex secretory program orchestrated by the inflammasome controls paracrine senescence. *Nat Cell Biol*. 2013; 15:978–90.
<https://doi.org/10.1038/ncb2784>

- PMID:[23770676](#)
56. Nelson G, Wordsworth J, Wang C, Jurk D, Lawless C, Martin-Ruiz C, von Zglinicki T. A senescent cell bystander effect: senescence-induced senescence. *Aging Cell*. 2012; 11:345–9. <https://doi.org/10.1111/j.1474-9726.2012.00795.x> PMID:[22321662](#)
57. Levi N, Papismadov N, Solomonov I, Sagi I, Krizhanovsky V. The ECM path of senescence in aging: components and modifiers. *FEBS J*. 2020; 287:2636–46. <https://doi.org/10.1111/febs.15282> PMID:[32145148](#)
58. Rashid K, Sundar IK, Gerloff J, Li D, Rahman I. Lung cellular senescence is independent of aging in a mouse model of COPD/emphysema. *Sci Rep*. 2018; 8:9023. <https://doi.org/10.1038/s41598-018-27209-3> PMID:[29899396](#)
59. Lagoumtzi SM, Chondrogianni N. Senolytics and senomorphics: Natural and synthetic therapeutics in the treatment of aging and chronic diseases. *Free Radic Biol Med*. 2021; 171:169–90. <https://doi.org/10.1016/j.freeradbiomed.2021.05.003> PMID:[33989756](#)
60. Franceschi C, Campisi J. Chronic inflammation (inflammaging) and its potential contribution to age-associated diseases. *J Gerontol A Biol Sci Med Sci*. 2014 (Suppl 1); 69:S4–9. <https://doi.org/10.1093/gerona/glu057> PMID:[24833586](#)
61. Lehallier B, Gate D, Schaum N, Nanasi T, Lee SE, Yousef H, Moran Losada P, Berdnik D, Keller A, Verghese J, Sathyan S, Franceschi C, Milman S, et al. Undulating changes in human plasma proteome profiles across the lifespan. *Nat Med*. 2019; 25:1843–50. <https://doi.org/10.1038/s41591-019-0673-2> PMID:[31806903](#)
62. Öhlund D, Handy-Santana A, Biffi G, Elyada E, Almeida AS, Ponz-Sarvise M, Corbo V, Oni TE, Hearn SA, Lee EJ, Chio II, Hwang CI, Tiriach H, et al. Distinct populations of inflammatory fibroblasts and myofibroblasts in pancreatic cancer. *J Exp Med*. 2017; 214:579–96. <https://doi.org/10.1084/jem.20162024> PMID:[28232471](#)
63. Huang J, Tsang WY, Li ZH, Guan XY. The Origin, Differentiation, and Functions of Cancer-Associated Fibroblasts in Gastrointestinal Cancer. *Cell Mol Gastroenterol Hepatol*. 2023; 16:503–11. <https://doi.org/10.1016/j.jcmgh.2023.07.001> PMID:[37451403](#)
64. Liu T, Han C, Wang S, Fang P, Ma Z, Xu L, Yin R. Cancer-associated fibroblasts: an emerging target of anti-cancer immunotherapy. *J Hematol Oncol*. 2019; 12:86. <https://doi.org/10.1186/s13045-019-0770-1> PMID:[31462327](#)
65. Qi J, Sun H, Zhang Y, Wang Z, Xun Z, Li Z, Ding X, Bao R, Hong L, Jia W, Fang F, Liu H, Chen L, et al. Single-cell and spatial analysis reveal interaction of FAP⁺ fibroblasts and SPP1⁺ macrophages in colorectal cancer. *Nat Commun*. 2022; 13:1742. <https://doi.org/10.1038/s41467-022-29366-6> PMID:[35365629](#)
66. Tommelein J, De Vlieghere E, Verset L, Melsens E, Leenders J, Descamps B, Debucquoy A, Vanhove C, Pauwels P, Gespach CP, Vral A, De Boeck A, Haustermans K, et al. Radiotherapy-Activated Cancer-Associated Fibroblasts Promote Tumor Progression through Paracrine IGF1R Activation. *Cancer Res*. 2018; 78:659–70. <https://doi.org/10.1158/0008-5472.CAN-17-0524> PMID:[29217764](#)
67. Rizzolio S, Giordano S, Corso S. The importance of being CAFs (in cancer resistance to targeted therapies). *J Exp Clin Cancer Res*. 2022; 41:319. <https://doi.org/10.1186/s13046-022-02524-w> PMID:[36324182](#)
68. Li H, Courtois ET, Sengupta D, Tan Y, Chen KH, Goh JLL, Kong SL, Chua C, Hon LK, Tan WS, Wong M, Choi PJ, Wee LJK, et al. Reference component analysis of single-cell transcriptomes elucidates cellular heterogeneity in human colorectal tumors. *Nat Genet*. 2017; 49:708–18. <https://doi.org/10.1038/ng.3818> PMID:[28319088](#)
69. Song M, He J, Pan QZ, Yang J, Zhao J, Zhang YJ, Huang Y, Tang Y, Wang Q, He J, Gu J, Li Y, Chen S, et al. Cancer-Associated Fibroblast-Mediated Cellular Crosstalk Supports Hepatocellular Carcinoma Progression. *Hepatology*. 2021; 73:1717–35. <https://doi.org/10.1002/hep.31792> PMID:[33682185](#)
70. Yoshimoto S, Loo TM, Atarashi K, Kanda H, Sato S, Oyadomari S, Iwakura Y, Oshima K, Morita H, Hattori M, Honda K, Ishikawa Y, Hara E, Ohtani N. Obesity-induced gut microbial metabolite promotes liver cancer through senescence secretome. *Nature*. 2013; 499:97–101. <https://doi.org/10.1038/nature12347> PMID:[23803760](#)
71. Yasuda T, Koiwa M, Yonemura A, Miyake K, Kariya R, Kubota S, Yokomizo-Nakano T, Yasuda-Yoshihara N, Uchihara T, Itoyama R, Bu L, Fu L, Arima K, et al.

- Inflammation-driven senescence-associated secretory phenotype in cancer-associated fibroblasts enhances peritoneal dissemination. *Cell Rep.* 2021; 34:108779.
<https://doi.org/10.1016/j.celrep.2021.108779>
PMID:33626356
72. Wang T, Notta F, Navab R, Joseph J, Ibrahimov E, Xu J, Zhu CQ, Borgida A, Gallinger S, Tsao MS. Senescent Carcinoma-Associated Fibroblasts Upregulate IL8 to Enhance Prometastatic Phenotypes. *Mol Cancer Res.* 2017; 15:3–14.
<https://doi.org/10.1158/1541-7786.MCR-16-0192>
PMID:27678171
73. Glabman RA, Choyke PL, Sato N. Cancer-Associated Fibroblasts: Tumorigenicity and Targeting for Cancer Therapy. *Cancers (Basel).* 2022; 14:3906.
<https://doi.org/10.3390/cancers14163906>
PMID:36010899
74. Pelka K, Hofree M, Chen JH, Sarkizova S, Pirl JD, Jorgji V, Bejnood A, Dionne D, Ge WH, Xu KH, Chao SX, Zollinger DR, Lieb DJ, et al. Spatially organized multicellular immune hubs in human colorectal cancer. *Cell.* 2021; 184:4734–52.e20.
<https://doi.org/10.1016/j.cell.2021.08.003>
PMID:34450029
75. Elyada E, Bolisetty M, Laise P, Flynn WF, Courtois ET, Burkhart RA, Teinor JA, Belleau P, Biffi G, Lucito MS, Sivajothi S, Armstrong TD, Engle DD, et al. Cross-Species Single-Cell Analysis of Pancreatic Ductal Adenocarcinoma Reveals Antigen-Presenting Cancer-Associated Fibroblasts. *Cancer Discov.* 2019; 9:1102–23.
<https://doi.org/10.1158/2159-8290.CD-19-0094>
PMID:31197017
76. Jia Y, Zhang B, Zhang C, Kwong DL, Chang Z, Li S, Wang Z, Han H, Li J, Zhong Y, Sui X, Fu L, Guan X, Qin Y. Single-Cell Transcriptomic Analysis of Primary and Metastatic Tumor Ecosystems in Esophageal Squamous Cell Carcinoma. *Adv Sci (Weinh).* 2023; 10:e2204565.
<https://doi.org/10.1002/advs.202204565>
PMID:36709495
77. Chen K, Wang Q, Li M, Guo H, Liu W, Wang F, Tian X, Yang Y. Single-cell RNA-seq reveals dynamic change in tumor microenvironment during pancreatic ductal adenocarcinoma malignant progression. *EBioMedicine.* 2021; 66:103315.
<https://doi.org/10.1016/j.ebiom.2021.103315>
PMID:33819739

SUPPLEMENTARY MATERIALS

Supplementary Figure



Supplementary Figure 1. Changes in expression of *CDKN1A*, *CDKN2A* and *LMNB1*, which are markers of senescence. Data represented are normalized gene expression values obtained from RNA sequencing data of non-senescent and senescent fibroblast lines from three subjects. *FDR≤0.001 versus NS using One-way ANOVA with Benjamini and Hochberg correction for false discovery rate.

Supplementary Tables

Please browse Full Text version to see the data of Supplementary Tables 2, 4 and 6.

Supplementary Table 1. Patient demographics for subject-derived fibroblast cell lines.

Cell Line#	Colon Location	Subject Age at time of tissue collection	Gender	Race	BMI	Smoking	NSAID	Diabetes	Use in study
NWBT3	Colon-Transverse	57	Male	White	33.67	Never	No	No	Validation by qPCR and Luminex
NWBT4	Sigmoid Colon	71	Male	White	35.61	Former	Yes	No	Validation by qPCR and Luminex
NWBT6	Sigmoid Colon	43	Male	Hawaiian/ Pacific Islander	32.74	Never	No	Type II	RNA Sequencing and validation by qPCR and Luminex
NWBT8	Sigmoid Colon	43	Female	Indian/Alaskan Native	47.72	Never	No	No	RNA Sequencing and validation by qPCR and Luminex
NWBT9	Rectosigmoid colon	55	Female	White	22.37	Former	NA	pre-diabetic	Validation by qPCR and Luminex
NWBT10	Sigmoid Colon	37	Male	White	25.9	Never	N/A	No	RNA Sequencing and validation by qPCR and Luminex
NWBT14	Colon	44	Female	White	19.8	Former	Yes	No	Validation by qPCR and Luminex

Supplementary Table 2. Core senescence profile in senescent primary human colon fibroblasts (Log2FoldChange ≥ 1 , FDR ≤ 0.01) after different oxidative and genotoxic stressors (versus non-senescent fibroblasts). Log2FoldChange values represent the average of primary lines derived from three different subjects.

Supplementary Table 3. KEGG analysis of the core senescence profile (FDR ≤ 0.05).

Pathway	n	count	p-value	fd	gene_ratio	pathway_id	genes
Lipid and atherosclerosis	215	11	8.17E-04	0.035859	5.116279	path:hsa05417	CYP1A1, CXCL1, CXCL2, CXCL8, MMP3, CCL2, CCL5, SOD2, VCAM1, CD36, CD40
Cytokine-cytokine receptor interaction	295	18	1.45E-06	1.27E-04	6.101695	path:hsa04060	TNFSF13B, CCR7, CXCL1, CXCL2, CXCL8, LIF, ACKR3, CCL2, CCL5, CCL20, CXCL5, CX3CL1, BMP2, TSLP, TNFRSF10C, GDF15, CXCL14, CD40
NF-kappa B signaling pathway	104	8	3.02E-04	0.015155	7.692308	path:hsa04064	TNFSF13B, CXCL1, CXCL2, BIRC3, CXCL8, RELB, VCAM1, CD40
Chemokine signaling pathway	192	15	5.38E-07	6.29E-05	7.8125	path:hsa04062	ADCY8, CCR7, SHC2, GRK4, CXCL1, CXCL2, CXCL8, SHC4, CCL2, CCL5, CCL20, CXCL5, CX3CL1, STAT1, CXCL14
IL-17 signaling pathway	94	8	1.50E-04	0.00877	8.510638	path:hsa04657	FOSB, CXCL1, CXCL2, CXCL8, MMP3, CCL2, CCL20, CXCL5
Epithelial cell signaling in Helicobacter pylori infection	70	6	9.92E-04	0.038676	8.571429	path:hsa05120	ATP6V0D2, CXCL1, CXCL2, CXCL8, F11R, CCL5
TNF signaling pathway	112	11	2.07E-06	1.45E-04	9.821429	path:hsa04668	CXCL1, CXCL2, BIRC3, LIF, MMP3, CCL2, CCL5, CCL20, CXCL5, CX3CL1, VCAM1
Malaria	50	5	0.001321	0.046365	10	path:hsa05144	CXCL8, CCL2, VCAM1, CD36, CD40

Rheumatoid arthritis	93	11	3.13E-07	5.50E-05	11.82796	path:hsa05323	TNFSF13B, CTSK, ATP6V0D2, CXCL1, CXCL2, CXCL8, MMP3, CCL2, CCL5, CCL20, CXCL5
Viral protein interaction with cytokine and cytokine receptor	100	12	7.53E-08	2.64E-05	12	path:hsa04061	CCR7, CXCL1, CXCL2, CXCL8, ACKR3, CCL2, CCL5, CCL20, CXCL5, CX3CL1, TNFRSF10C, CXCL14

Supplementary Table 4A. Gene ontology analysis for biological processes on the core senescence profile (FDR ≤ 0.01).

Supplementary Table 4B. Organization of gene ontologies to remove redundancies. GO terms in *bold* are represented in Figure.

Supplementary Table 5. GO analysis for molecular function on the core senescence profile (FDR ≤ 0.01).

GO ID	Pathway	Fold enrichment	Enrichment FDR	N genes	Pathway genes	Gene ratio	Genes
GO:0030545	Signaling receptor regulator activity	3.99	0.0000137	21	629	3.339	CX3CL1 TG CXCL2 TNFSF13B CCL2 CCL20 BMP2 LIF FGF13 GDF15 GPNMB TSLP CXCL14 STC1 CXCL5 CXCL1 CXCL8 LYNX1 CDNF CCK CCL5
GO:0005102	Cytokine/chemokine receptor binding	2.11	0.0004620	40	1722	2.323	CX3CL1 TG CXCL2 TNFSF13B PLAT CCL2 CPE CCL20 ITGB6 STAT1 IGFBP2 C3 BMP2 FGL2 LIF FGF13 SHC2 GDF15 CD36 GPNMB GABARAPL1 TSLP CXCL14 F11R STC1 SQSTM1 SHANK1 VCAM1 CXCL5 CXCL1 TAC3 BDKRB2 NSG1 CXCL8 LYNX1 CDNF PRKN SHC4 CCK CCL5
GO:0030414	Peptidase inhibitor activity	5.12	0.0013185	10	204	4.902	BIRC3 CST4 RENBP C3 SNCA SERPINI1 SPINT1 CST2 CST1 PROS1
GO:0046873	Metal ion transmembrane transporter activity	3.03	0.0035773	16	454	3.524	SLC4A7 SLC6A15 TMEM38A SLC1A2 SLC6A12 KCNJ2 KCNC3 KCNK1 KCNJ6 KCNH6 SCN4B SCN5A KCNK12 TPCN1 RYR2
GO:0005216	Ion channel activity	3.05	0.0044680	15	459	3.268	TMEM38A P2RX6 KCNJ2 KCNC3 KCNK1 CLCA2 KCNJ6 KCNH6 SCN4B SCN5A KCNK12 TPCN1 RYR2 TMEM150C
GO:0043394	Proteoglycan binding	8.65	0.0072366	5	38	13.158	CFH GPNMB CTSK CTSS HPSE2
GO:0005215	Transporter activity	1.92	0.0082971	31	1364	2.273	SLC4A7 SLC6A15 TMEM38A SLC7A8 P2RX6 ATP8B4 SLC16A6 SLC1A2 SLC6A12 CNNM1 KCNJ2 ABCC4 KCNC3 CD36 KCNK1 SLCO2B1 CLCA2 SLC44A3 SLC2A12 ATP6V0D2 ABCA9 KCNJ6 KCNH6 SCN4B SCN5A KCNK12 TPCN1 APOD RYR2 TMEM150C

GO:0005153	Interleukin-8 receptor binding	50.18	0.0087442	2	3	66.667	CX3CL1 CXCL8
GO:0005283	Amino acid:sodium symporter activity	16.73	0.0117724	3	14	21.429	SLC6A15 SLC1A2 SLC6A12
GO:0008028	Monocarboxylic acid transmembrane transporter activity	6.78	0.0144993	5	59	8.475	SLC16A6 SLC6A12 ABCC4 CD36 SLCO2B1
GO:0005416	Amino acid:cation symporter activity	15.05	0.0144993	3	18	16.667	SLC6A15 SLC1A2 SLC6A12
GO:0004930	G protein-coupled receptor activity	3.02	0.0182516	11	1026	1.072	CELSR3 LPAR2 ADGRB2 CCR7 ACKR3 BDKRB2 GPRC5C LPAR3 CMKLR1 ADGRB1 ADGRL1
GO:0005516	Calmodulin binding	3.20	0.0182516	10	208	4.808	DAPK2 MAP2 WFS1 IQGAP2 OBSCN ADCY8 RRAD CAMK1D SCN5A RYR2
GO:0047655	Allyl-alcohol dehydrogenase activity	33.45	0.0182516	2	4	50.000	AKR1B1 AKR1B10
GO:0005342	Organic acid transmembrane transporter activity	3.79	0.0182791	8	161	4.969	SLC6A15 SLC7A8 SLC16A6 SLC1A2 SLC6A12 ABCC4 CD36 SLCO2B1
GO:0001637	G protein-coupled chemoattractant receptor activity	11.58	0.0259279	3	26	11.538	CCR7 ACKR3 CMKLR1
GO:0070915	Lysophosphatidic acid receptor activity	25.09	0.0304585	2	5	40.000	LPAR2 LPAR3
GO:0005343	Organic acid:sodium symporter activity	10.75	0.0312890	3	28	10.714	SLC6A15 SLC1A2 SLC6A12
GO:0008061	Chitin binding	20.07	0.0457024	2	8	25.000	OVGP1 CHI3L1
GO:0008131	Primary amine oxidase activity	20.07	0.0457024	2	6	33.333	AOC2 VCAM1
GO:0038023	Signaling receptor activity	1.82	0.0467353	23	1940	1.186	CELSR3 LPAR2 NOTCH3 GPC4 P2RX6 CD40 ITGB6 NR4A3 ADGRB2 CCR7 CD36 LEF1 ACKR3 NR4A2 BDKRB2 GPRC5C LPAR3 TNFRSF10C CMKLR1 ADGRB1 ROBO2 L1CAM ADGRL1

Supplementary Table 6A. GO analysis for biological processes on the Core senescence SASP subset (FDR ≤ 0.01).

Supplementary Table 6B. GO analysis for molecular function on the Core senescence SASP subset (FDR ≤ 0.05).

Supplementary Table 7. Comparison of the core colon fibroblast senescence profile to an aging associated secretome described by Lehallier et al. (2019).

Gene symbol	ENSEMBL ID	H2O2 Induced Senescence vs. NS		Doxo - Induced Senescence vs. NS		Bleo - Induced Senescence vs. NS		Data from Lehallier et al. 2019		
		Average Log2FC	Adjusted p	Average Log2FC	Adjusted p	Average Log2FC	Adjusted p	p.Age	q.Age	Coefficient. Age
ADSSL1	ENSG00000185100	2.159	8.659E-16	1.591	1.714E-08	1.663	1.187E-08	7.998E-14	7.670E-13	0.0019
C1QTNF1	ENSG00000173918	1.286	1.551E-09	1.569	2.063E-13	1.746	5.610E-16	6.924E-13	6.175E-12	0.0006
CCL5	ENSG00000271503	2.148	4.320E-03	3.641	1.862E-07	3.623	6.261E-07	6.808E-09	4.425E-08	0.0017
CD36	ENSG00000135218	2.155	3.529E-08	2.520	1.151E-10	1.762	3.537E-05	2.628E-32	6.570E-31	0.0018
CDNF	ENSG00000185267	2.475	2.186E-06	2.149	7.549E-05	1.874	1.368E-03	1.264E-11	1.022E-10	0.0008
CHI3L1	ENSG00000133048	2.245	2.173E-07	1.949	1.280E-05	2.310	4.067E-07	1.695E-35	4.677E-34	0.0051

CXCL1	ENSG00000163739	1.606	6.344E-04	2.436	8.507E-08	3.009	6.272E-11	6.191E-06	2.790E-05	0.0009
CXCL14	ENSG00000145824	2.218	8.181E-06	2.738	2.307E-08	2.194	3.307E-05	1.321E-02	3.029E-02	0.0004
CXCL8	ENSG00000169429	3.214	1.242E-03	4.262	1.194E-05	4.168	4.430E-05	6.932E-08	3.937E-07	0.0008
DAPK2	ENSG00000035664	1.852	4.034E-05	1.916	2.512E-05	1.568	1.517E-03	1.376E-03	4.004E-03	0.0009
GABARAPL1	ENSG00000139112	1.057	4.308E-04	1.056	5.056E-04	1.008	1.624E-03	2.010E-10	1.484E-09	0.0016
GDF15	ENSG00000130513	3.399	1.335E-04	3.777	2.136E-05	3.235	6.352E-04	2.333E-252	1.706E-249	0.0053
GPNMB	ENSG00000136235	1.818	4.733E-38	1.034	2.892E-12	1.114	1.843E-13	1.486E-05	6.335E-05	0.0007
HK2	ENSG00000159399	1.202	2.245E-03	1.201	2.501E-03	1.249	2.593E-03	3.369E-03	9.058E-03	0.0013
LICAM	ENSG00000198910	2.268	1.437E-07	1.812	5.562E-05	1.343	6.625E-03	3.875E-05	1.524E-04	0.0005